Nanostructures

DOI: 10.1002/anie.201204829

A Yolk–Shell Nanoreactor with a Basic Core and an Acidic Shell for Cascade Reactions**

Yan Yang, Xiao Liu, Xiaobo Li, Jiao Zhao, Shiyang Bai, Jian Liu, and Qihua Yang**

Cascade reactions, which allow a consecutive series of chemical reactions to proceed in a concurrent fashion, have attracted intensive research attention owing to their high atom economy, step-saving and biomimetic nature.[1] For efficiently catalyzing a cascade reaction, the fabrication of solid catalysts with precise control over the location of different functionalities is generally required but still a great challenge.[2] In comparison with the solid catalysts without well-defined morphology, the yolk–shell nanoparticles (YSNs) with unique core@void@shell nanostructure are promising candidates as nanoreactors for cascade reactions owing to the easy functionalization of both the core and the shell, the high density of exposed active sites endowed by the movable core, and the protection effect endowed by the shell, especially under harsh reaction conditions.[3] Significantly, since each core in the YSNs is isolated by a permeable shell and has a relatively homogeneous environment, in principle, the catalytically active sites could be accurately located in the core or on the shell. This arrangement provides the possibility to design and fabricate solid nanoreactors for cascade reactions.[4]

However, the YSNs reported to date are generally composed of a catalytically active core, such as metal, metal oxide, and alloy nanoparticles, with inert shell, which limited their further applications as nanoreactors in cascade reactions. The synthesis of YSNs with precisely located active sites both in the core and on the shell is no easy task and has rarely been reported, though various synthesis methods have been developed, including ship-in-bottle approach, soft templating approaches, template-free approaches, Ostwald ripening or galvanic replacement processes, and methods based on the Kirkendall effect.[5]

Recently, a facile organosilane-assisted etching method has been developed by our group to fabricate YSNs based on the in situ formation of the shell and partially or completely etching the predefined core.[6] A unique feature of this method is the possibility to precisely functionalize the core and shell step-by-step by using the versatile sol–gel chemistry. By using this method, the catalytic functionalities including even incompatible groups, such as acidic and basic groups, could be located in a controlled manner either in the core or on the shell of YSNs. Herein, we present the fabrication of YSNs with basic core ($-NH_2$) and acidic shell ($-SO_3H$) by an organosilane-assisted selective etching method. The catalytic efficiency of these YSNs as nanoreactors for catalyzing the deacetalization–Henry cascade reaction was demonstrated. This synthetic method has been extended to the synthesis of various functionalized YSNs and YSNs with multilayered shells, thus providing a general approach for the fabrication of multifunctional nanoreactors.

The overall process for the synthesis of YSNs with basic core and acidic shell is illustrated in Figure 1 A (for synthesis details see Section S4 of the Supporting Information). Initially, spherical mesoporous silica nanospheres (MSNs)

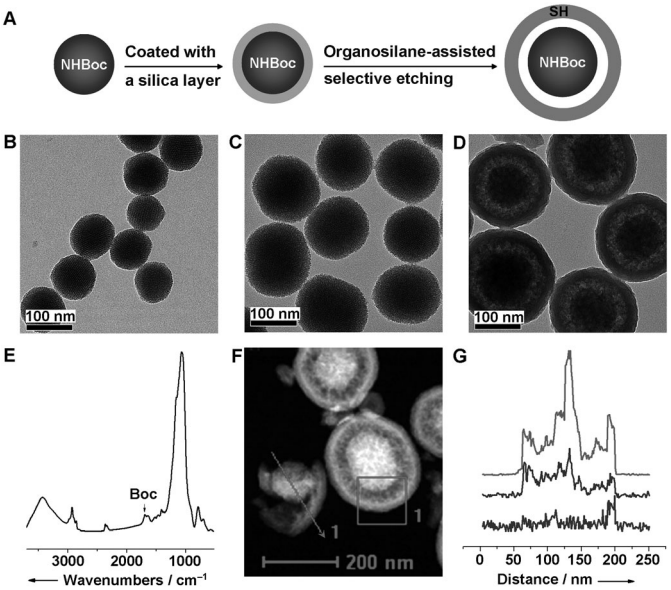

Figure 1. A) Schematic illustration showing the general procedure for the synthesis of YS-NHBoc@SH with NHBoc in the core and SH on the shell (NHBoc = $NHOCOC(CH_3)_3$); B, C) TEM images of NHBoc-functionalized mesoporous silica nanospheres before (B) and after (C) coating with a sacrificial silica layer; D) TEM image of YS-NHBoc@SH obtained by treatment of the sample in (C) with BTME and MPTMS; E) FTIR spectrum of YS-NHBoc@SH; F) HAADF-STEM image of YS-NHBoc@SH after treatment with H_2PtCl_6 and $PdCl_2$ (before the treatment with $PdCl_2$, the sample was treated in vacuum at 150°C to convert the NHBoc groups into NH_2 groups); and G) EDX analysis along the line shown in (F) of a broken nanosphere that was chosen intentionally. The upper, middle, and lower traces correspond to Si, Pd (magnified by a factor of 9), and Pt (magnified by a factor of 10), respectively.

[*] Y. Yang, Dr. X. Liu, X. B. Li, Dr. J. Zhao, Dr. S. Y. Bai, Dr. J. Liu, Prof. Q. H. Yang
State Key Laboratory of Catalysis
Dalian Institute of Chemical Physics
Chinese Academy of Sciences
457 Zhongshan Road, Dalian 116023 (China)
E-mail: yangqh@dicp.ac.cn
Homepage: http://www.hmm.dicp.ac.cn

[**] The authors would like to thank the National Natural Science Foundation of China (20923001) and the National Basic Research Program of China (2009CB623503) for the financial support.

Supporting information for this article is available on the WWW under http://dx.doi.org/10.1002/anie.201204829.

functionalized with 3-*tert*-butyloxycarbonylaminopropyl groups were prepared by co-condensation of 3-*tert*-butyloxycarbonylaminopropyltriethoxysilane and tetraethoxysilane (TEOS) in the presence of cetyltrimethyl-ammonium bromide (CTAB) in NaOH aqueous solution according to a modified Stöber method.[7] The average particle size is around 100 nm based on the transmission electron microscopy (TEM) image (Figure 1B). After the hydrolysis and condensation of TEOS catalyzed by ammonia, the nanospheres were covered with a silica layer with a thickness of 22 nm (Figure 1C). The subsequent addition of 1,2-bis(trimethoxysilyl)ethane (BTME) and (3-mercaptopropyl)trimethoxysilane (MPTMS) into the synthesis system resulted in the formation of YS-NHBoc@SH with a yolk–shell nanostructure. As shown in Figure 1D, YS-NHBoc@SH has a shell thickness of around 20 nm and the void between core and shell is approximately 24 nm, thus suggesting that only the silica layer around the parent NHBoc-MSNs was selectively etched during the organosilane-assisted etching process. This finding suggests that the silica layer acts as a sacrificial layer to protect the core and the dissolution of the silica layer generates the void space between the core and the shell.

The successful incorporation of NHBoc groups in YS-NHBoc@SH was verified by FTIR spectroscopy (Figure 1E). The location of the functional groups in YS-NHBoc@SH after selective coordination of Pt^{4+} and Pd^{2+} ions to SH and NH_2 groups, respectively, was characterized by TEM, high angular annular dark-field scanning transmission electron microscopy (HAADF-STEM), and energy-dispersive X-ray spectrometry (EDX; for experimental details see Section S5 of the Supporting Information). The HAADF-STEM image (Figure 1F) of the resulting YS-NH_2-Pd^{2+}@SH-Pt^{4+} provides a clear contrast of the core, the hollow part, and the porous shell. The EDX elemental analysis of a broken sample shows the hollow region between the core and shell, with the core rich in Pd and the shell rich in Pt, thereby confirming that NH_2 and SH groups are mainly located in the core and on the shell, respectively (Figure 1F and G). The successful location of different types of functional groups in YSNs is attributed to the separate steps for core and shell formation and the protection effect of the sacrificial silica layer covering the initial nanospheres. Thus, it is possible to precisely locate the active sites in the core or on the shell of YSNs through controlled addition of functional groups at different synthetic steps.

YS-NH_2@SO_3H with basic core and acidic shell can be facilely obtained through post-treatment of YS-NHBoc@SH by oxidation of the SH to SO_3H groups using H_2O_2 and deprotection of the NHBoc to NH_2 groups[2b,8] (for experimental details see Section S6 of the Supporting Information). The HRTEM image of YS-NH_2@SO_3H clearly shows the uniform distribution of the monodispersed YSNs with a core size of 100 nm, a void space between the core and the shell of approximately 20 nm, and a shell thickness of approximately 20 nm (Figure 2A). 2-D hexagonal arrangement of the mesopores in the core and the existence of the open mesopores on the shell are observed, which is quite important to facilitate the mass diffusion of the guest molecules through the YSNs. The appearance of one strong diffraction peak between 1–3° in the XRD pattern proves that YS-NH_2@SO_3H has an ordered mesostructure (Figure S1 in the Supporting Information), which is consistent with the TEM result. The SEM image verifies that YS-NH_2@SO_3H is composed of uniform and monodispersed nanospheres with an average particle size of 190 nm (Figure 2B). The nitrogen adsorption–desorption isotherm of YS-NH_2@SO_3H displays a typical type-IV isotherm with a two-step capillary condensation in the relative pressure range of 0.1–0.3 and 0.5–0.9 (Figure S2 in the Supporting Information); this type of isotherm is in agreement with the presence of a hierarchical porosity organization of the yolk–shell nanostructure.[5k] YS-NH_2@SO_3H has a BET surface area of 178 $m^2 g^{-1}$, a pore volume of 0.30 $cm^3 g^{-1}$, and a pore diameter of 2.4 nm (Table S1 in the Supporting Information). The above characterizations suggest that the morphology, structure, and physical parameters of YS-NH_2@SO_3H are identical to those of YS-NHBoc@SH (Figure 1D; Figure 2A; Table S1 in the Supporting Information), thus showing that YS-

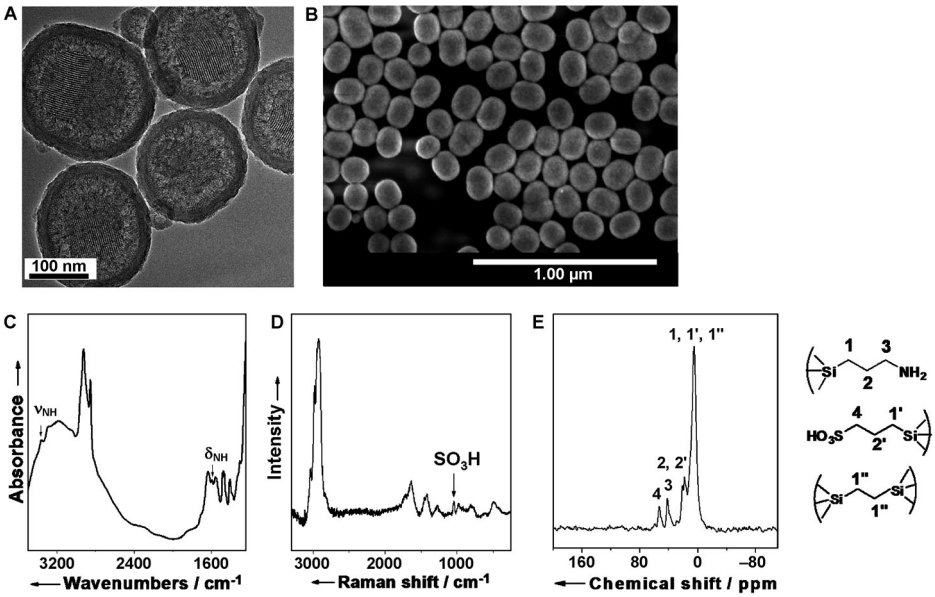

Figure 2. Characterization results of YSNs with basic cores and acidic shells (YS-NH_2@SO_3H). A) TEM image, B) SEM image, C) FTIR spectrum, D) UV-Raman spectrum, and E) ^{13}C cross-polarization magic-angle spinning (CP/MAS) NMR spectrum of YS-NH_2@SO_3H.

NHBoc@SH is robust enough to survive the post-treatment process.

The chemical composition of YS-NH_2@SO_3H was verified by FTIR, UV-Raman, and NMR spectroscopy (Figure 2C–E). The FTIR spectrum of YS-NH_2@SO_3H displays characteristic peaks at 2958–2854 cm^{-1} assigned to CH vibrations of bridging ethylene and propyl groups, and 1596 cm^{-1} attributed to NH vibration of amine groups (Figure 2C).[9] The existence of sulfonic acid groups was confirmed by the vibration at 1045 cm^{-1} in the UV-Raman spectrum of YS-NH_2@SO_3H (Figure 2D).[8] The ^{13}C CP/MAS NMR spectrum of YS-NH_2@SO_3H displays the signals at $\delta = 53.4$ and 42.0 ppm assigned to the carbon atoms bonded to sulfonic acid and amine groups, respectively (Figure 2E),[2b] thereby confirming the existence of amine and sulfonic acid groups. The solid-state ^{29}Si NMR spectrum of YS-NH_2@SO_3H (Figure S3 in the Supporting Information) shows the characteristic resonances in the range of $\delta = -103$ to -112 ppm and $\delta = -57$ to -67 ppm, which are attributed to Q and T silicon species, respectively. The above characterizations further confirm the successful incorporation of NH_2 and SO_3H functional groups in the YSNs. YS-NH_2@SO_3H exhibits an amino content of 240 $\mu mol\,g^{-1}$ and acidic exchange capacity of 80 $\mu mol\,g^{-1}$. This result shows that YS-NH_2@SO_3H has both acidic and basic functionalities (Table S1 in the Supporting Information).

The above synthetic approach provides an easy route towards the fabrication of YSNs with precise control over the location of various active sites. The synthesis of YS-silica@-SO_3H (pure silicate core with SO_3H groups on the shell) and of YS-NH_2@ethanesilica (amine groups in the core and ethylene-bridged organosilica shell) has been successfully demonstrated (for experimental details see Section S7 of the Supporting Information). The TEM images show that both samples have a similar yolk–shell nanostructure and identical particle size and core size as YS-NH_2@SO_3H (Figure S4 in the Supporting Information). The successful incorporation of sulfonic acid and amine groups in YS-silica@SO_3H and YS-NH_2@ethanesilica, respectively, was further confirmed by FTIR and UV-Raman spectroscopy (Figure S5 in the Supporting Information), thereby showing the generality of this method for the fabrication of YSNs with precise location of the functional groups. YS-silica@SO_3H and YS-NH_2@ethanesilica have identical pore diameters of 2.4 nm with BET surface areas of 157 and 239 $m^2\,g^{-1}$, respectively (Table S1 in the Supporting Information).

Similar to the synthesis of YS-NH_2@SO_3H, YS-silica@-ethanesilica (pure silica core and ethylene-bridged organosilica shell; for synthesis details see Section S8 of the Supporting Information) can also be obtained by using mesoporous silica nanospheres as initial material (MSNs) and BTME as the organosilane source (Figure 3A). YS-silica@ethanesilica has an average particle size of 190 nm, a core size of 110 nm, and a void space between the core and the shell of approximately 20 nm based on the SEM and TEM images (Figure S6 in the Supporting Information and Figure 3B). The spherical core of YS-silica@ethanesilica has a highly ordered 2-D hexagonal mesostructure as evidenced by XRD and TEM results (Figure S7 in the Supporting Information and Figure 3B). A control experiment shows that the direct addition of BTME to the synthesis medium of the MSNs (without deposition of a silica layer) can result in the formation of yolk–shell nanostructures with rough surfaces and disorderly structured cores (Figure S8 in the Supporting Information). The presence of the silica sacrificial layer is an essential element that ensures the core retains the original mesostructure and remains discrete.

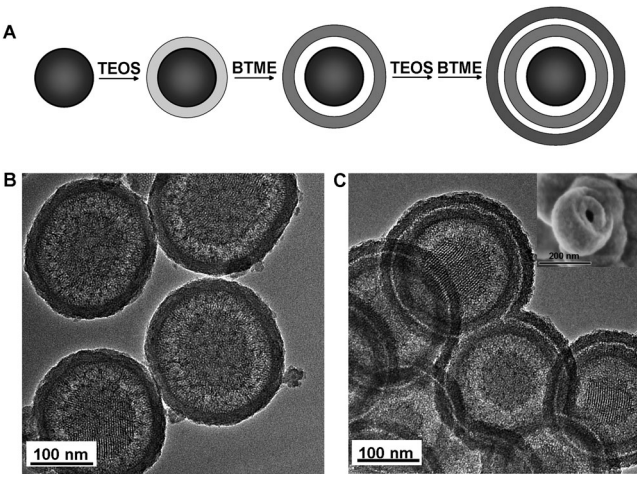

Figure 3. Synthetic process and TEM characterizations of YSNs with one and two shells. A) Schematic illustration showing the strategy to YSNs with one and two shells; TEM images of B) YS-silica@ethanesilica with a single shell and C) YS-silica@ethanesilica@ethanesilica with two shells (the inset shows the SEM image, scale bar is 200 nm).

A repetition of the synthesis process would yield yolk–shell nanoparticles with multiple shells (Figure 3C). To prepare YSNs with two shells (YS-silica@ethanesilica@ethanesilica), YS-silica@ethanesilica was selected as seed, and the addition of TEOS and BTME was repeated as shown in Figure 3A (for synthesis details see Section S8 of the Supporting Information). YS-silica@ethanesilica@ethanesilica with a particle size of 240 nm is composed of two mesoporous shells with shell thicknesses of 40 nm and an interlayer space of 5–6 nm, a void space between the core and shell, and the mesoporous core with highly ordered structure (Figure 3C). The SEM image of the broken nanosphere that was chosen intentionally after mechanical fracturing, further confirms the double-shelled nanostructure (inset of Figure 3C). The existence of the strong diffraction peak in the XRD pattern confirms the ordered organization of the mesopores in the core; this result is consistent with the TEM result (Figure S9 in the Supporting Information). The nitrogen sorption isotherm shows a type-IV isotherm with two hysteresis loops at relative pressure values P/P_0 of 0.2–0.4 and 0.5–0.8 that correspond to the mesopores of 2.4 nm in the core and shell and the interlayer space of 5.8 nm, respectively (Figure S10 in the Supporting Information); this result further confirms the double-shelled structure. The doubled-shelled YSNs exhibit high BET surface areas of 708 $m^2\,g^{-1}$ with a total pore volume of 0.81 $cm^3\,g^{-1}$ (Table S1 in the Supporting Information). It is believed that YSNs with an ordered mesoporous core and multiple shells can also be synthesized

by repeating the coating and etching steps. Hence, the versatility of this synthesis strategy towards the fabrication of YSNs with well-located active sites, controllable shell layers and compositions, and complex hollow structures has been successfully demonstrated.

The catalytic performance of YS-NH_2@SO_3H was tested in the deacetalization–Henry cascade reaction and compared with that of YS-NH_2@ethanesilica and YS-silica@SO_3H (Table 1). The deacetalization reaction is firstly catalyzed by the SO_3H groups, followed by the Henry reaction catalyzed by the amine groups. Thus only the co-existence of acidic and basic groups could catalyze the reaction smoothly. No reaction occurs in the presence of YS-NH_2@ethanesilica, and only the deacetalization product is observed using YS-silica@SO_3H. As expected, the cascade reaction can be efficiently catalyzed by YS-NH_2@SO_3H with high activity (100% conversion) and selectivity (100%). This finding suggested that acid on the shell and base in the core are efficiently separated by the unique yolk–shell nanostructure, without neutralization. The mixture of YS-NH_2@ethanesilica and YS-silica@SO_3H can also catalyze the reaction with 55% conversion under the same reaction conditions (the content of NH_2 and SO_3H in different catalysts is shown in Table S1 in the Supporting Information). Based on the reaction profiles, the mixture of YS-NH_2@ethanesilica and YS-silica@SO_3H exhibits a much lower reaction rate than YS-NH_2@SO_3H (turnover frequency (TOF): 6 versus 13 h^{-1}; Figure 4A). The reaction route to explain the high activity of YS-NH_2@SO_3H is depicted in Figure 4B. The reactant (benzaldehyde dimethyl acetal) diffuses through the porous shell, and its conversion into benzaldehyde is catalyzed by -SO_3H groups on the shell. The intermediate benzaldehyde diffuses further into the core and is converted into the final product, nitrostyrene; this reaction is catalyzed by the -NH_2 groups located in the core. The integration of both the acidic and basic functional groups in one nanoreactor could shorten the reaction pathway. Thus the much lower catalytic activity of the physical mixture than of YS-NH_2@SO_3H is mainly due to the long diffusion route from one acidic nanoreactor to the other basic one. Furthermore, YS-NH_2@SO_3H shows 100% conversion with quantitative yield of the final product for 4-methyl and 4-nitro-benzaldehyde dimethyl acetal and 77% conversion with 65% yield of the final product for 4-chlorobenzaldehyde dimethyl acetal (Table S2 in the Supporting Information). The high yield and selectivity of YS-NH_2@SO_3H suggest that the appropriate location of the active sites in the YSNs is essential to make different kinds of functional groups work efficiently during the catalytic process, especially for the ones that are incompatible with each other.

Table 1: Deacetalization–Henry cascade reaction catalyzed by different catalysts.[a]

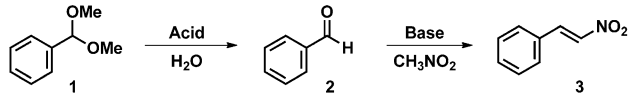

Catalyst	Conv. of **1** [%]	Yield of **2** [%][b]	Yield of **3** [%][b]	TOF [h^{-1}]
YS-silica@SO_3H	100	>99	trace	–
YS-NH_2@ethanesilica	trace	trace	trace	–
YS-NH_2@ethanesilica + YS-silica@SO_3H[c]	55	trace	55	6
YS-NH_2@SO_3H	100	trace	>99	13
YS-NH_2@SO_3H 2nd[d]	100	12	88	–
YS-NH_2@SO_3H 3rd[d]	100	28	72	–

[a] Reaction conditions: benzaldehyde dimethyl acetal (0.5 mmol), solid catalyst (0.025 mmol of amine), CH_3NO_2 (5 mL), 90°C, 22 h. [b] Determined by GC analysis using nitrobenzene as internal standard. [c] Physical mixture of YS-NH_2@ethanesilica and YS-silica@SO_3H containing the same amount of amine and acid as YS-NH_2@SO_3H. [d] The second or third recycled catalysts.

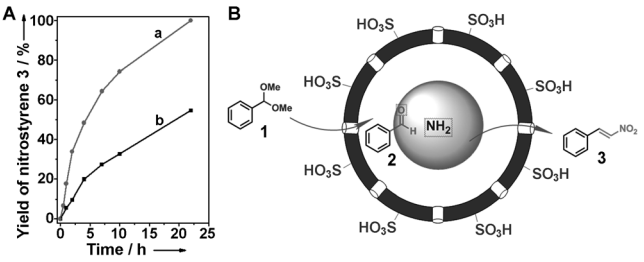

Figure 4. Catalytic performance of the YSN nanoreactor. A) The reaction profiles of YS-NH_2@SO_3H (a), and the mixture (b) of YS-NH_2@ethanesilica and YS-silica@SO_3H for the deacetalization–Henry cascade reaction. B) Schematic illustration of the cascade reaction in a YS-NH_2@SO_3H nanoreactor.

YS-NH_2@SO_3H can be recycled and exhibits 100% conversion with 88% and 72% yield of nitrostyrene for the second cycle and third cycle, respectively (Table 1). The TEM characterization (Figure S11 A in the Supporting Information) shows that the used YS-NH_2@SO_3H still has a well-defined yolk–shell nanostructure but the structural order of the core was deteriorated. The slight decrease in the yield of nitrostyrene (catalyzed by amine groups) is probably due to the deteriorated structural order of the core.

In summary, we demonstrated the facile synthesis of YSNs with controllable chemical compositions, spatial locations of functional groups, and tuneable shell layers. Through the organosilane-assisted selective etching method, various functionalized YSNs with well-located active sites, both in the core and on the shell, that included the active functional groups -NH_2, -SH, and -SO_3H, were synthesized, and the location of the functional groups was clearly characterized. By introducing amine and sulfonic acid groups into the cores and onto the shells, respectively, the yolk–shell nanoreactors with isolated acidic and basic active sites in one nanoreactor were obtained for the first time, and showed high catalytic activity in a one-pot deacetalization–Henry cascade reaction. It can be envisioned that YSNs with various well-located active sites, controllable shell layers and chemical compositions could also be synthesized through this strategy. The spatial isolation effect presented herein may open up new opportunities for the applications of multiple functionalized YSNs as efficient nanoreactors for catalysis.

Received: June 20, 2012
Published online: August 2, 2012

Keywords: cascade reactions · yolk–shell nanoparticles · acid–base nanoreactors · nanostructures

[1] a) C. Grondal, M. Jeanty, D. Enders, *Nat. Chem.* **2010**, *2*, 167 – 178; b) M. Climent, A. Corma, S. Iborra, M. Mifsud, *J. Catal.* **2007**, *247*, 223 – 230; c) K. C. Nicolaou, J. S. Chen, *Chem. Soc. Rev.* **2009**, *38*, 2993 – 3009; d) R. J. R. W. Peters, I. Louzao, J. C. M. van Hest, *Chem. Sci.* **2012**, *3*, 335 – 342; e) D. M. Vriezema, M. C. Aragones, J. Elemans, J. Cornelissen, A. E. Rowan, R. J. M. Nolte, *Chem. Rev.* **2005**, *105*, 1445 – 1489; f) C. Zhao, J. A. Lercher, *Angew. Chem.* **2012**, *124*, 6037 – 6042; *Angew. Chem. Int. Ed.* **2012**, *51*, 5935 – 5940.

[2] a) A. Katz, M. E. Davis, *Nature* **2000**, *403*, 286 – 289; b) J. Alauzun, A. Mehdi, C. Reye, R. J. P. Corriu, *J. Am. Chem. Soc.* **2006**, *128*, 8718 – 8719; c) N. T. S. Phan, C. S. Gill, J. V. Nguyen, Z. J. Zhang, C. W. Jones, *Angew. Chem.* **2006**, *118*, 2267 – 2270; *Angew. Chem. Int. Ed.* **2006**, *45*, 2209 – 2212; d) D. M. Vriezema, P. M. L. Garcia, N. Sancho Oltra, N. S. Hatzakis, S. M. Kuiper, R. J. M. Nolte, A. E. Rowan, J. C. M. van Hest, *Angew. Chem.* **2007**, *119*, 7522 – 7526; *Angew. Chem. Int. Ed.* **2007**, *46*, 7378 – 7382; e) A. L. Miller, N. B. Bowden, *Adv. Mater.* **2008**, *20*, 4195 – 4199; f) F. Zhang, G. H. Liu, W. H. He, H. Yin, X. S. Yang, H. Li, J. Zhu, H. X. Li, Y. F. Lu, *Adv. Funct. Mater.* **2008**, *18*, 3590 – 3597; g) S. Shylesh, A. Wagener, A. Seifert, S. Ernst, W. R. Thiel, *Angew. Chem.* **2010**, *122*, 188 – 191; *Angew. Chem. Int. Ed.* **2010**, *49*, 184 – 187; h) K. Motokura, N. Fujita, K. Mori, T. Mizugaki, K. Ebitani, K. Kaneda, *J. Am. Chem. Soc.* **2005**, *127*, 9674 – 9675.

[3] a) X. W. Lou, L. A. Archer, Z. Yang, *Adv. Mater.* **2008**, *20*, 3987 – 4019; b) J. Liu, S. Z. Qiao, J. S. Chen, X. W. Lou, X. Xing, G. Q. Lu, *Chem. Commun.* **2011**, *47*, 12578 – 12591; c) J. Liu, S. Z. Qiao, Q. H. Hu, G. Q. Max Lu, *Small* **2011**, *7*, 425 – 443; d) R. Ghosh Chaudhuri, S. Paria, *Chem. Rev.* **2012**, *112*, 2373 – 2433; e) F. Q. Tang, L. L. Li, D. Chen, *Adv. Mater.* **2012**, *24*, 1504 – 1534.

[4] a) P. M. Arnal, M. Comotti, F. Schüth, *Angew. Chem.* **2006**, *118*, 8404 – 8407; *Angew. Chem. Int. Ed.* **2006**, *45*, 8224 – 8227; b) Q. Zhang, T. R. Zhang, J. P. Ge, Y. D. Yin, *Nano Lett.* **2008**, *8*, 2867 – 2871; c) S. H. Joo, J. Y. Park, C.-K. Tsung, Y. Yamada, P. Yang, G. A. Somorjai, *Nat. Mater.* **2009**, *8*, 126 – 131; d) Q. Zhang, I. Lee, J. P. Ge, F. Zaera, Y. D. Yin, *Adv. Funct. Mater.* **2010**, *20*, 2201 – 2214; e) B. Liu, W. Zhang, H. L. Feng, X. L. Yang, *Chem. Commun.* **2011**, *47*, 11727 – 11729; f) X. L. Fang, Z. H. Liu, M.-F. Hsieh, M. Chen, P. X. Liu, C. Chen, N. F. Zheng, *ACS Nano* **2012**, *6*, 4434 – 4444; g) D. A. Wilson, R. J. M. Nolte, J. C. M. van Hest, *Nat. Chem.* **2012**, *4*, 268 – 274; h) S. Wu, J. Dzubiella, J. Kaiser, M. Drechsler, X. H. Guo, M. Ballauff, Y. Lu, *Angew. Chem.* **2012**, *124*, 2272 – 2276; *Angew. Chem. Int. Ed.* **2012**, *51*, 2229 – 2233.

[5] a) K. Kamata, Y. Lu, Y. N. Xia, *J. Am. Chem. Soc.* **2003**, *125*, 2384 – 2385; b) Y. D. Yin, R. M. Rioux, C. K. Erdonmez, S. Hughes, G. A. Somorjai, A. P. Alivisatos, *Science* **2004**, *304*, 711 – 714; c) D. M. Cheng, X. D. Zhou, H. B. Xia, H. S. O. Chan, *Chem. Mater.* **2005**, *17*, 3578 – 3581; d) Y. Vasquez, A. K. Sra, R. E. Schaak, *J. Am. Chem. Soc.* **2005**, *127*, 12504 – 12505; e) H. M. Chen, R. S. Liu, K. Asakura, J. F. Lee, L. Y. Jang, S. F. Hu, *J. Phys. Chem. B* **2006**, *110*, 19162 – 19167; f) D. K. Yi, S. S. Lee, G. C. Papaefthymiou, J. Y. Ying, *Chem. Mater.* **2006**, *18*, 614 – 619; g) H. X. Li, Z. F. Bian, J. Zhu, D. Q. Zhang, G. S. Li, Y. N. Huo, H. Li, Y. F. Lu, *J. Am. Chem. Soc.* **2007**, *129*, 8406 – 8407; h) X. W. Lou, C. Yuan, L. A. Archer, *Adv. Mater.* **2007**, *19*, 3328 – 3332; i) X. J. Wu, D. S. Xu, *J. Am. Chem. Soc.* **2009**, *131*, 2774 – 2775; j) Y. Chen, H. R. Chen, L. M. Guo, Q. J. He, F. Chen, J. Zhou, J. W. Feng, J. L. Shi, *ACS Nano* **2010**, *4*, 529 – 539; k) J. Liu, S. Z. Qiao, S. B. Hartono, G. Q. Lu, *Angew. Chem.* **2010**, *122*, 5101 – 5105; *Angew. Chem. Int. Ed.* **2010**, *49*, 4981 – 4985; l) X. J. Wu, D. S. Xu, *Adv. Mater.* **2010**, *22*, 1516 – 1520; m) M. Ibáñez, J. Fan, W. Li, D. Cadavid, R. Nafria, A. Carrete, A. Cabot, *Chem. Mater.* **2011**, *23*, 3095 – 3104; n) L. Kuai, S. Wang, B. Geng, *Chem. Commun.* **2011**, *47*, 6093 – 6095.

[6] Y. Yang, J. Liu, X. B. Li, X. Liu, Q. H. Yang, *Chem. Mater.* **2011**, *23*, 3676 – 3684.

[7] J. Kim, H. S. Kim, N. Lee, T. Kim, H. Kim, T. Yu, I. C. Song, W. K. Moon, T. Hyeon, *Angew. Chem.* **2008**, *120*, 8566 – 8569; *Angew. Chem. Int. Ed.* **2008**, *47*, 8438 – 8441.

[8] J. S. Gao, J. Liu, S. Y. Bai, P. Wang, H. Zhong, Q. H. Yang, C. Li, *J. Mater. Chem.* **2009**, *19*, 8580 – 8588.

[9] L. Zhang, J. Liu, J. Yang, Q. H. Yang, C. Li, *Microporous Mesoporous Mater.* **2008**, *109*, 172 – 183.

